Path-Permutation Codes for End-to-End Transmission in Ad Hoc Cognitive Radio Networks

I-Wei Lai, *Member, IEEE*, Chia-Han Lee, *Member, IEEE*, Kwang-Cheng Chen, *Fellow, IEEE*, and Ezio Biglieri, *Life Fellow, IEEE*

***Abstract*—Cognitive radios (CRs) improve the spectrum efficiency in wireless communications. Nonetheless, owing to the intrinsic randomness of *ad hoc* cognitive radio networks (CRNs), e.g., the opportunistic links, the traditional realization of *ad hoc* networking that demands the end-to-end control information, is unscalable and impractical. A virtual multiple-input multiple-output (MIMO) framework has been recently developed for the realization of error-resilient end-to-end transmission without the necessity of feedback information. In this paper, we propose an end-to-end path-permutation coded (PPC) transmission in which one relay path is accessed at a time and the transmission is hopped among multiple relay paths. The hopping order is specified by a permutation array that encodes the data, meaning that the data is conveyed by the order of indices of the accessed paths. With the PPC scheme, the control overhead and data processing complexity of the end-to-end transmission become relatively low. The PPC technique can also be utilized as a multiuser technique. At the destination node, a joint sphere decoder efficiently implements the maximum *a posteriori* (MAP) probability decoding that simultaneously identifies the order of accessed paths and erasures. Comprehensive theoretical analyses and simulations are conducted to demonstrate the superior performance of the PPC technique in ad hoc CRNs.**

***Index Terms*—Cognitive radio network (CRN), ad hoc network, erasure channel, permutation code, error rate analysis, Meijer G-function, sphere decoder.**

I. Introduction

COGNITIVE RADIO (CR) has been widely regarded as a key technology to enhance the spectrum utilization in wireless communications [1]–[5]. While a primary user has the highest priority to access licensed channels, a CR is designed to dynamically adapt its parameters to exploit the available spectrum without interfering in a relevant way with primary users. Ad hoc cognitive radio networks (CRNs), which are formed by primary users and CRs, aim at improving the end-to-end communication performance without centralized control.

A. Problem Statement

Let the *link* denote the connection between two nodes, and *path* the end-to-end connection route between a pair of source and destination nodes. Although spectrum efficiency is greatly enhanced by employing the CR, the CR links are opportunistic, and hence cause random transmission outage owing to mainly three reasons: First, to avoid interfering with other users, a relay node has to sense the availability of the opportunistic CR link to its next node before forwarding. However, practically vulnerable spectrum sensing results in collisions or severe interference when a node forwards CR packets to a link occupied by other users. Second, even with perfect spectrum sensing, the end-to-end transmission latency may be increased due to the link unavailability, especially when the spectrum is heavily used. For the CR packets experiencing a long transmission delay beyond their lifetime, they are discarded before arriving at the destination node [6], resulting in the transmission outage. Last, the deep fading may also cause the links opportunistic. Under this circumstance, tremendous efforts are required to establish and maintain the control channel and feedback link. For example, many routing algorithms have been proposed for the purpose of precise control of ad hoc CRNs, which generally require end-to-end information. However, since the opportunistic links are random, unreliable and thus likely unidirectional [6], [7], the construction of a feedback link and a reliable control channel for the end-to-end information exchange demands tremendous control overhead. Such control overhead limits the scalability of the algorithms to a large ad hoc CRN [8]–[12].

B. Related Work

Alternatively, routing can be established in a *statistical* manner by utilizing only the local information [13]–[15], meaning that some links in a route are allowed to be available occasionally such that the control overhead can be greatly saved. To combat the negative effects of intrinsic randomness in this routing, error-resilient end-to-end transmission should be developed [12], [16]. In the context of the multipath routing [17]–[19], the *virtual multiple-input multiple-output (MIMO)* technology at the network/session layer is proposed [20]–[22].

Manuscript received May 2, 2014; revised October 27, 2014; accepted January 28, 2015. Date of publication February 13, 2015; date of current version June 6, 2015. The work of Ezio Biglieri was supported by the Project TEC2012-34642. The work of Chia-Han Lee was supported by the Ministry of Science and Technology (MOST) under the grant MOST103-2221-E-001-002. This research is supported in part by the Ministry of Science and Technology, National Taiwan University, and Intel Corp. under Grants MOST 102-2221-E-002-016-MY2, MOST 103-2911-I-002-001, NTU ICRP-104R7501. The associate editor coordinating the review of this paper and approving it for publication was A. Kwasinski.

I-W. Lai is with the Research Center for Information Technology Innovation, Academia Sinica, Taipei 115, Taiwan (e-mail: iweilai0924@gmail.com).

C.-H. Lee is with the Research Center for Information Technology Innovation, Academia Sinica, Taipei 115, Taiwan (e-mail: chiahan@citi.sinica.edu.tw).

K.-C. Chen is with the Graduate Institute of Communication Engineering, National Taiwan University, Taipei 10617, Taiwan (e-mail: chenkc@cc.ee.ntu.edu.tw).

E. Biglieri is with Universitat Pompeu Fabra, Barcelona 08002, Spain, and also with University of California at Los Angeles (UCLA), Los Angeles, CA 90095 USA (e-mail: e.biglieri@ieee.org).

Color versions of one or more of the figures in this paper are available online at http://ieeexplore.ieee.org.

Digital Object Identifier 10.1109/TWC.2015.2403848

By encoding packets along both path and time coordinates, error-resilient end-to-end transmission without feedback information is realized by using the path-time code (PTC) [20], [21]. The main idea of PTC is to transmit multiple coded packets using all the relay paths and jointly decode them at the destination node.

Although the superiority of the PTC has been demonstrated, this technique may not be suitable for all kinds of ad hoc CRNs, due to several of its features. First, all the relay paths in the multipath routing are concurrently accessed by the CR user using the PTC technique. The availability of the opportunistic links in the ad hoc CRN is thus reduced, especially when the number of CR users and/or relay paths used by each CR user is large. Second, the control overhead due to multiple access is introduced, if CR users utilizing overlapped multipath routes need to transmit simultaneously. The control overhead also arises from the synchronization of the multiple coded packets transported in different relay paths to make them arrive at the destination node within the same time period. Third, at the destination node, joint decoding of multiple PTC coded packets is a burden for a CRN whose nodes have a limited processing power. Consequently, when the ad hoc CRN with numerous power-limited CRs requires to support multiuser transmission, a different technique is called for to efficiently provide reliable end-to-end transmission. *Path-permutation coding* (PPC), to be described in this paper, is one such technique.

C. Introduction of PPC

Instead of simultaneously transmitting multiple packets through multiple relay paths, end-to-end multipath PPC transmission only accesses one relay path at a time. This accessed path is selected based on the data sequence in the packet. Specifically, PPC encodes the data packet in two ways, i.e., by using the *transmitted symbols* with quadrature amplitude modulation (QAM) and by using a *permutation array* (PA) consisting of a set of path indices. The term *permutation code* comes from the fact that the PPC code word comprises these PAs. Consider a toy example of PPC using two relay paths and two time instants. In addition to the bits conveyed by the transmitted QAM symbols, the source node can encode another bit with PAs {12} and {21}. Specifically, if the bit '0' is encoded by the PAs, the first and the second relay paths are successively selected at the first and second time instants according to the PA {12}. Contrarily, if this bit value is '1', the second and the first relay paths are successively selected at the first and second time instants according to the PA {21}. The destination node then identifies the order of the accessed paths and decodes the transmitted QAM symbols to recover the data packet.

The proposed end-to-end PPC transmission enjoys several advantages as follows:

1) **Error resilience**: The PPC code word is dispersed through various time instants, creating the time diversity that allows the data packet to be recovered if a transmission outage occurs at some time instants and/or some relay paths. With reference to the previous toy example, the destination node is able to recover the data even if data is only successfully transmitted through one path. It follows that the end-to-end PPC transmission is robust to the presence of randomly available opportunistic links.
2) **High link availability**: Since one relay path is used at each time instant in the context of end-to-end PPC transmission, link availability of the ad hoc CRN in this case is higher than that of the end-to-end PTC transmission where all relay paths in the multipath routing are concurrently accessed.
3) **Multiple access**: With the assigned PAs, multiple CRs can transmit simultaneously, and thus the PPC can be utilized as a multiple access technique in multiuser scenarios.
4) **Low control overhead**: Since only one packet is transmitted at a time, the multiplexing technique or the two-step protocol [23] for the transmission at the source node is saved. Also, the control for the synchronization of the arrival of multiple coded packets is avoided.
5) **Low encoding and decoding complexity**: Since the encoding only performs the selection of the relay path, the encoding complexity is low. Decoding the single PPC-coded packet which includes the identification of the order of the accessed paths, i.e., the PA, is much simpler than the joint decoding of multiple PTC-coded packets.

In this work, we develop the framework of end-to-end PPC transmission. The erasure channel model is used to describe the random transmission outage caused by the effects mentioned previously: the packet loss due to long transmission latency, the deep fading, and the vulnerable spectrum sensing which results in severe interference or collisions [21]. At the source node, the data packet is encoded by the PAs of the path indices along the time coordinate. The Hamming distances between PPC code words and the number of encoded bits depend on the size of the adopted PA set. Thus, data rate and reliability can be flexibly traded by using various PA sets with different sizes. To achieve a deeper understanding of PPC, we study the pairwise error probability (PEP) of end-to-end PPC transmission. In multihop ad hoc CRNs, the equivalent fading gain of the relay path is the product of link gains, i.e., the product of multiple complex random variables, which complicates the theoretical error rate analysis. In this paper, bit error rate (BER), capacity, and BER floor at high signal-to-noise ratio (SNR) under various link availability scenarios are provided. In addition, we develop an efficient multiple-tree joint sphere decoding (JSD) algorithm operating at the destination node, which jointly identifies the presence of erasures and the order of the accessed paths so as to decode the data packet.

The rest of this paper is organized as follows: Section II describes the virtual MIMO system and reviews end-to-end PTC transmission. Section III elaborates on the proposed end-to-end PPC transmission and its extension to multiple access in multiuser scenarios. Section IV analyzes the performance of end-to-end PPC transmission. Section V introduces the optimal decoding algorithm. Section VI provides numerical results to validate the analysis and to demonstrate the performance of the proposed end-to-end PPC transmission. Finally, conclusions are drawn in Section VII.

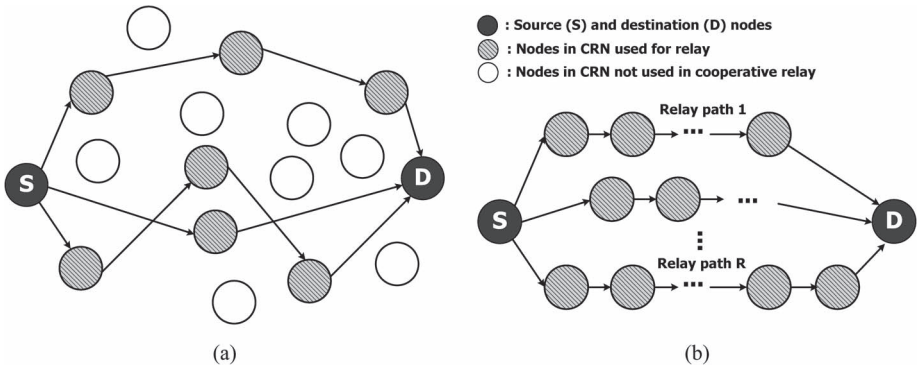

Fig. 1. Example topology of the multipath end-to-end transmission in an ad hoc multihop CRN. (a) Topology of a multihop ad hoc CRN. (b) Equivalent directed graph model.

II. System Model and End-to-End PTC Transmission

The ad hoc CRN with multihop multipath route [17]–[19] can be viewed as a set of R link-disjoint paths [16], [24], each of them comprising $N_r - 1$, for $r = 1, \ldots, R$, relay nodes. Fig. 1(a) illustrates an example of the network topology of the constructed multipath routes, while Fig. 1(b) depicts an equivalent directed-graph model. To describe the virtual MIMO system and for the comparison with the PPC technique, in this section we review the end-to-end PTC transmission.

A. Erasure Channel Model

After establishing the multiple relay paths, the PTC-coded packets are transmitted to different relay paths. The coded packet in each relay path is then amplified and forwarded towards the destination node. When the packet relaying between the nodes experience a long end-to-end transmission latency, the packet is discarded, thus causing an *erasure*. Erasures also occur due to deep fading or to the imperfection of spectrum sensing, which results in severe interference or collisions when the coded packet is forwarded to a link occupied by the primary or other CR users. Let us define M as the number of discrete-time instants used to transmit a data packet. The erasure pattern is described by an *erasure matrix* $\mathbf{V} \in \{0,1\}^{M \times R}$ whose (m,r)th entry $v_{m,r}$ is a Bernoulli random variable [25] taking value '0' when an erasure occurs at the rth path and the mth time instant, and value '1' when the rth relay path is available at the bth time instant.

We now analytically compute the erasure statistics due to long end-to-end delay. The probability of the path availability $P(v_{m,r} = 1)$ depends on the waiting period W_m and the number of opportunistic links N_r. Specifically, during the end-to-end transmission, each node performs sensing at the beginning of every sensing interval. The waiting period W_m (normalized with respect to the sensing interval) indicates the overall number of sensing attempts that the nodes are allowed to perform for the sequential N_r opportunistic links in a path [21] at time instant b as illustrated in Fig. 2.

Sequential sensing of N_r opportunistic links can be modeled as a Bernoulli trial, characterized by the geometrically distributed random variable $G(\delta)$, where δ is the probability of a link being unavailable. Assuming that the transmission latency is relatively small compared with the delay caused by the unavailability of occupied links, the end-to-end delay is the summation of N_r geometric random variables. Consequently, this normalized delay τ with respect to the sensing interval follows a negative binomial distribution $\mathrm{NB}(N_r, \delta)$ with probability mass function (PMF) [16]

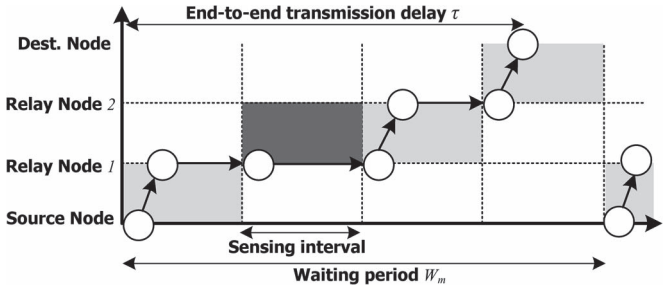

Fig. 2. Illustration of the relationship among sensing interval, waiting period, and the end-to-end delay with an example of $W_m = 4$ and $N_r = 3$. The circles indicate the transmitted coded packet at time instant m. The dark grey square indicates the unavailable link, while the light grey squares indicate the available links. In this example, we have $v_{m,r} = 1$ since the end-to-end delay is shorter than the waiting period.

$$P_{\mathrm{NB}}(\tau; N_r, \delta) = \binom{\tau + N_r - 1}{N_r - 1} (1-\delta)^{N_r} \delta^{\tau}. \quad (1)$$

When such end-to-end delay τ is smaller than or equal to the waiting period W_m, the coded packet can be successfully transmitted through the rth relay path at the bth time instant. Consequently, the probability of path availability (i.e., $v_{m,r} = 1$) is given by [16]

$$P(v_{m,r}=1) = P(\tau \le W_m) = \sum_{\tau=N_r}^{W_m} P_{\mathrm{NB}}(\tau - N_r; N_r, \delta). \quad (2)$$

When the erasures due to deep fading and severe interference are considered, the erasure probability $P(v_{m,r} = 0) = 1 - P(v_{m,r} = 1)$ computed here can be used as the lower bound. This erasure statistics is essential for the performance analysis in Section IV and the design of JSD at the destination node, which is introduced in Section V.

B. End-to-End PTC Transmission

To perform end-to-end PTC transmission, the source node encodes a data packet $\mathbf{x} \in \chi^M$ using the coding matrix $\tilde{\mathbf{C}}_m \in \mathbb{C}^{R\times M}$, where χ denotes the QAM constellation set. The resulting coded packet $\tilde{\mathbf{C}}_m\mathbf{x}$ is transmitted at time instant m. Let $\mathbf{v}_m = [v_{m,1}, \ldots, v_{m,R}]^\top$ be the erasure vector of R paths at time b, where $(\cdot)^\top$ denotes the transposition. Define $\mathbf{h}_m = [h_{m,1}, \ldots, h_{m,R}]^\top \in \mathbb{C}^R$ as the path fading vector at time b, and the Schur product of $\mathbf{h}_m$ and $\mathbf{v}_m$ as $\mathbf{h}_m \circ \mathbf{v}_m = [h_{m,1}v_{m,1}, \ldots, h_{m,R}v_{m,R}]^\top$. The received coded packet at the destination node has the form

$$\begin{aligned} y_m &= (\mathbf{h}_m \circ \mathbf{v}_m)^\top \tilde{\mathbf{C}}_m\mathbf{x} + \sum_{r=1}^{R} \tilde{n}_{m,r} \\ &= (\mathbf{h}_m \circ \mathbf{v}_m)^\top \tilde{\mathbf{C}}_m\mathbf{x} + n_m, \end{aligned} \tag{3}$$

where $\tilde{n}_{m,r}$ denotes the additive white Gaussian noise (AWGN) aggregated from all links in the rth path at time instant b. Since $\tilde{n}_{m,r}$ has a variance depending on the pair (m, r) due to the amplification of the opportunistic link gains [23], the AWGN n_m has a time-varying power spectral density, denoted by $N_{0,m}$.

The received coded packet from $m = 1$ to $m = M$ can be represented as

$$\begin{aligned} \mathbf{y} &= \begin{bmatrix} (\mathbf{h}_1 \circ \mathbf{v}_1)^\top & \ldots & \mathbf{0}^\top \\ \vdots & \ddots & \vdots \\ \mathbf{0}^\top & \ldots & (\mathbf{h}_M \circ \mathbf{v}_M)^\top \end{bmatrix} \underbrace{\begin{bmatrix} \tilde{\mathbf{C}}_1 \\ \vdots \\ \tilde{\mathbf{C}}_M \end{bmatrix}}_{\mathbf{C}} \mathbf{x} \\ &\quad + \underbrace{\begin{bmatrix} n_1 \\ \vdots \\ n_M \end{bmatrix}}_{\mathbf{n}} = \underbrace{\begin{bmatrix} (\mathbf{h}_1 \circ \mathbf{v}_1)^\top \tilde{\mathbf{C}}_1 \\ \vdots \\ (\mathbf{h}_M \circ \mathbf{v}_M)^\top \tilde{\mathbf{C}}_M \end{bmatrix}}_{\mathbf{H}_{\mathrm{eq}}(\mathrm{V},\mathrm{C})} \mathbf{x} + \mathbf{n} \\ &= \mathbf{H}_{\mathrm{eq}}(\mathrm{V}, \mathrm{C})\mathbf{x} + \mathbf{n}, \end{aligned} \tag{4}$$

where $\mathbf{C} = [\tilde{\mathbf{C}}_1^\top \ \ldots \ \tilde{\mathbf{C}}_M^\top]^\top \in \mathbb{C}^{RM\times M}$ represents the cascaded $\tilde{\mathbf{C}}_m$. With the formulation in (4), the end-to-end coded transmission in *ad hoc* CRNs is described by the same mathematical expression as a MIMO system, characterized by the equivalent channel matrix $\mathbf{H}_{\mathrm{eq}}(\mathbf{V}, \mathbf{C}) \in \mathbb{C}^{M\times M}$. This MIMO matrix incorporates the RM Bernoulli random variables modeling the erasures, and can be modified by a suitable choice of the coding scheme [26, p. 350 ff.]. In other words, (4) can be interpreted as describing a virtual MIMO system where multiple nodes are coordinated to form the multihop/multipath route between a source/destination node pair. The source node encodes the data packet along time and path coordinates, thus generating $\mathbf{H}_{\mathrm{eq}}(\mathbf{V}, \mathbf{C})$. At the destination node, multiple PTC-coded packets successfully arriving at the destination from various time slots and relay paths are first collected. Next, since the destination does not have an *a priori* knowledge of the erasure pattern, joint detection is performed to simultaneously identify the entries of $\mathbf{V}$, i.e., the erasures, and decode the data packet $\mathbf{x}$.

PTC exploits path and time diversity to increase the end-to-end transmission reliability [20], [21]. For the discrete Fourier transform (DFT)-based PTC [21], the (k, m)th entry of the coding matrix, $C_{k,m}$, takes the form

$$C_{k,m} = \frac{1}{\sqrt{R}} e^{\frac{-j2\pi km}{RM}},\ k = 1, \ldots, RM,\ m = 1, \ldots, M. \tag{5}$$

The use of DFT matrices as coding matrices has several advantages. In particular, since $\mathbf{C}$ comprises nonzero elements, every x_m is dispersed through all the R relay paths and all the M time instants. As long as $\mathbf{v}_m \neq \mathbf{0}$, all entries of the mth row vector of $\mathbf{H}_{\mathrm{eq}}(\mathbf{V}, \mathbf{C})$ are nonzero. Thus, $\mathbf{x}$ is received unerased at time b, which results in increased diversity [21]. Additionally, given two different vectors $\mathbf{x}$ and $\tilde{\mathbf{x}}$, the associated Hamming distance of the PTC-coded packets can be maximized to RM. The DFT-based PTC allows efficient implementation by fast Fourier transform (FFT) architectures, as those in wide use with orthogonal frequency-division multiplexing (OFDM) systems.

When the PTC is applied, it can be seen that multiple coded packets are concurrently transmitted through multiple relay paths, thus providing error-resilient end-to-end transmission. However, this mechanism simultaneously occupies R opportunistic links, which implies that the link availability decreases quickly, especially when the number of CR users and/or R is large. What is even worse, when CR users with overlapped routes need to transmit simultaneously, multiple-access techniques are required, which introduces undesired control overhead. Unavoidable control overhead also arises from the synchronization allowing multiple coded packets transmitted through different relay paths to arrive at the destination node within the same time frame. Last, considering the computational complexity of the PTC decoding at the destination node, joint decoding of multiple PTC coded packets is a burden for destination nodes possessing limited processing power. The search space for the joint detection of $(\mathbf{x}, \mathbf{V})$ has cardinality $2^{MR}|\chi|^M$, which is up to 1.6×10^7 for the case of $R = M = 4$ and QPSK ($|\chi| = 4$). To overcome these drawbacks, the PPC is proposed as an alternative technique for end-to-end transmission in ad hoc CRNs.

III. End-to-End PPC Transmission and PPC-Based Multiple Access

In this section, end-to-end PPC transmission in ad hoc CRNs is elaborated upon, including its encoding mechanism and the corresponding virtual MIMO formulation. Then, we generalize the end-to-end PPC transmission to a multiuser scenario where multiple CR users with overlapped multipath routes can concurrently transmit by properly using different PAs.

A. Encoding of PPC

We first denote $\mathcal{C}_R$ as the PA set which comprises all the possible $R!$ permutations of R objects. For example, for $R = 3$, we have $3! = 6$ length-three permutations, i.e.,

$$\mathcal{C}_3 = \{123, 132, 213, 231, 312, 321\}. \tag{6}$$

Next, we define the Hamming distance matrix $\mathbf{D}$ whose (i, j)th component $d_{i,j}$ is the Hamming distance between the ith and

TABLE I
PA SUBSETS PROPOSED IN [27] AND USED IN THIS PAPER

R	$\log_2 K$	$d_{\min}$	$\mathcal{C}_R(K, d_{\min})$	Mapping
3	2	2	231, 213, 132, 123	DIM
4	4	2	1234, 1243, 1324, 1342, 1423, 1432, 2134, 2143, 3214, 3241, 2314, 2341, 3421, 3412, 3124, 2341	DCM
	3	3	1234, 1342, 1423, 3241, 4132, 2314, 2431, 2143	DIM
	2	4	1234, 2341, 3412, 4123	DIM
5	4	3	12345, 13452, 14523, 15234 23514, 25143, 21435, 24351, 31542, 32154, 34215, 35421, 52413, 53241, 51324, 54132	DIM
6	4	4	123456, 213654, 421365, 132564, 241536, 435216, 624513, 145623, 264351, 452631, 543162, 362415, 354126, 615432, 536421, 316524	DIM

the jth permutation. For example, the Hamming distance matrix of $\{231, 213, 132, 123\} \subset \mathcal{C}_3$ is

$$\begin{bmatrix} 0 & 2 & 2 & 3 \\ 2 & 0 & 3 & 2 \\ 2 & 3 & 0 & 2 \\ 3 & 2 & 2 & 0 \end{bmatrix}, \tag{7}$$

a symmetric matrix with null diagonal entries. The minimum Hamming distance of the PA, $d_{\min}$, is the smallest off-diagonal entry of $\mathbf{D}$, i.e.,

$$d_{\min} = \min_{\substack{i,j=1,\ldots,K \\ i \neq j}} d_{i,j}, \tag{8}$$

so that $2 \leq d_{\min} \leq R$.

With these notations, let $\mathcal{C}_R(K, d_{\min}) \subset \mathcal{C}_R$ denote a subset of $\mathcal{C}_R$ including K PAs with minimum Hamming distance $d_{\min}$, which is known at both the source and destination nodes for the encoding and decoding. This PA subset can be assigned off-line and periodically updated. The two parameters K and $d_{\min}$ respectively reflect data rate and reliability, since PPC maps a data sequence with length of $\log_2 K$ bits one-to-one to a permutation in $\mathcal{C}_R(K, d_{\min})$. The larger K is, the more bits can be encoded by this PA subset, but the value of the minimum Hamming distance may get smaller. As illustrated in Table I, $d_{\min}$ decreases as K increases, which implies that the *rate-reliability* tradeoff can be flexibly adjusted by appropriately choosing these parameters.

Various permutation subsets and their mapping rules, e.g., distance-conserving mapping (DCM) and distance-increasing mapping (DIM), are addressed in [27]. For the DCM, the Hamming distance between any pairs of PAs may be the same or larger than that of their associated demapped binary data, while for the DIM, the Hamming distance between the PA pairs is guaranteed to larger to the distance between the associated demapped binary data. Considering the case of $R = 4$ illustrated in Table I, while the DCM provides $(\log_2 K, d_{\min}) = (4, 2)$, the DIM provides $(\log_2 K, d_{\min}) = (2, 3)$ which improves the reliability at the expense of lower throughput.

We now explain the encoding of PPC. In this work we focus on the case $M = R$, but the extension to the more general case $R \neq M$ is straightforward. Given the user requirements and the system parameters, a PA subset $\mathcal{C}_R(K, d_{\min})$ is selected and known by both the source and the destination nodes. Then, the PPC encoder encodes parts of the data to a permutation $\mathbf{r} = [r_1, \ldots, r_M] \in \mathcal{C}_R(K, d_{\min})$ such that the r_mth path is accessed at the mth time instant for the end-to-end PPC transmission. S constellation points $\mathbf{x} = [x_1, \ldots, x_S] \in \chi^S$, which are also used to encode the data in addition to those conveyed by the PA $\mathbf{r}$, are sequentially transmitted through different relay paths at M time instants with $1 \leq S \leq M$. In this case, the coding matrix $\tilde{\mathbf{C}}_m \in \{0, 1\}^{R \times S}$ comprises only one nonzero entry at the (r_m, s)th position with value "1" that assigns x_s to the r_mth relay path. Consequently, the PPC can be considered a special case of the PTC. In the following, we only consider the simplest case with $S = 1$ which is already sufficient to demonstrate the superiority of the PPC. For $S = 1$, $\mathbf{x}$ in the virtual MIMO system model (4) is reduced to a scalar x, while the coding matrix is reduced to a vector $\mathbf{c} \in \{0, 1\}^{RM}$ where the subvector $\tilde{\mathbf{c}}_m \in \{0, 1\}^R$ has only one nonzero term in the r_m position, i.e.,

$$\tilde{c}_{m,j} = \begin{cases} 1, & \text{if } j = r_m, \\ 0, & \text{otherwise.} \end{cases} \tag{9}$$

The virtual MIMO system model in (4) of the end-to-end PPC transmission thus simplifies to

$$\mathbf{y} = (\mathbf{h_r} \circ \mathbf{v_r})x + \mathbf{n}, \tag{10}$$

where, with some abuse of notation, we define $\mathbf{h_r} = [h_{1,r_1}, \ldots, h_{M,r_M}] \in \mathbb{C}^M$ to represent the fading of the selected path from time instant 1 to M; $\mathbf{v_r} = [v_{1,r_1}, \ldots, v_{M,r_M}] \in \{0, 1\}^M$ is defined similarly. It should be emphasized that certain relay paths may be occupied by the primary users for a long duration. By hopping among various relay paths, the end-to-end PPC transmission can easily overcome this problem. Since only one transmission occurs on a single relay path at each time instant, some control overhead, e.g., the control overhead for the synchronization of the arrival of multiple coded packets, of the end-to-end PTC transmission can be saved. Additionally, the relay paths do not need to be link-disjoint, because only one path is accessed at a time. The multipath routes can thus be established more easily.

B. Comparison of PTC and PPC in Multiuser Ad Hoc CRNs

For the conventional multipath end-to-end transmission, e.g., flooding with a repetition code or PTC, CR users concurrently access all relay paths to improve the rate-reliability tradeoff. However, due to the concurrent access of multiple relay paths, the availability of the opportunistic links in the ad hoc CRN decreases, and hence erasures occur more frequently. Even worse, as shown in Fig. 3 for the case of two CR users sharing the same multipath route, only a single user is permitted to perform the end-to-end transmission when flooding or PTC methods are used. Multiple access techniques, causing undesired control overhead, are needed for multiuser transmission.

Contrarily, at each time instant, the end-to-end PPC transmission only accesses one relay path even when multiple relay paths are available. Therefore, the availability of opportunistic links in the ad hoc CRN is higher than with the conventional end-to-end multipath transmission, thus leading to smaller

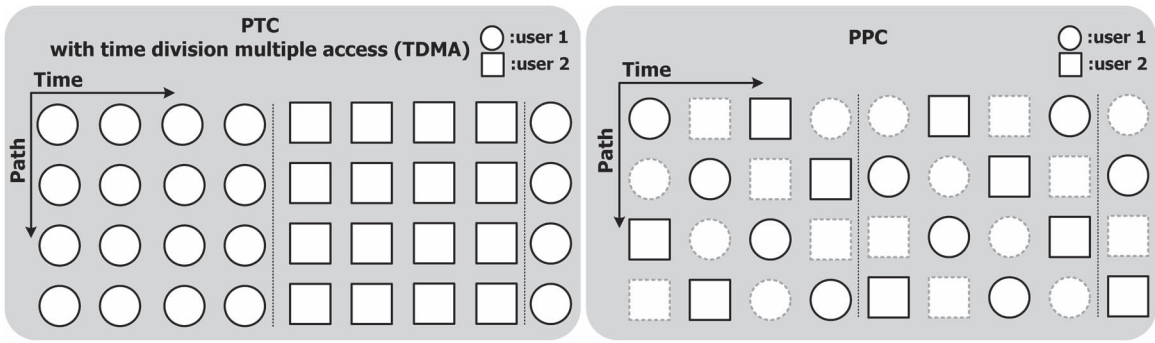

Fig. 3. A two-user, four-relay-path example for end-to-end transmission using PTC and PPC. Nine time instants are shown. While PTC requires multiple-access techniques to allow multiple users to utilize the overlapped routes, the PPC technique supports multiple access directly. The squares and circles respectively indicate the paths and time instants reserved to user 1 and user 2. For the PPC, the user 1 uses PA {1234} and {2341} to encode bit '0' and bit '1', while the user 2 adopts PA {3412} and {4123} to encode bit '0' and bit '1'. In this example, both the user 1 and user 2 encode bit '0' and bit '1' on the path indices respectively at the time instants 1 to 4 and at the time instants 5 to 8. The solid squares and circles indicate the paths and time instants where the user 1 and user 2 respectively select to perform the end-to-end transmission, according to the PAs.

erasure probabilities of CRN. Moreover, by generalizing the PPC technique, multiple users can concurrently utilize the overlapped multipath routes. Consider again the example in Fig. 3. For the end-to-end PPC transmission, different sets of permutations {1234, 2341} and {3412, 4123} can be respectively assigned to user 1 and user 2. Since the minimum Hamming distance between these two permutation subsets remains 4, which is identical to R, these two CR users can transmit simultaneously without interfering with each other.

The multiple access supporting higher throughput requirement with acceptable interference among users can also be realized by using the PPC technique. Specifically, if the minimum Hamming distance $d_{\min}$ between the permutation subsets adopted by various CR users is smaller than R, the throughput can be increased but collisions between the coded packets of various users may occur, which gives rise to an erasure. Fortunately, thanks to the intrinsic robustness to the outage of the end-to-end PPC transmission, these collisions can be resolved by the PPC decoders at destination nodes. The end-to-end PPC transmission thus generalizes the rate-reliability tradeoff to *user-rate-reliability tradeoff*, which can also support different throughput requirements of multiple users by assigning various sizes of permutation sets off-line and updating the permutation sets periodically. Up to R CR users can concurrently operate without interfering with each other in a certain R-path route. It should be emphasized that, the example given in Fig. 3 is the special case where the multiple CR users share the same multipath route for the illustration purpose. Practically, different CR users may have routes with only some opportunistic links shared. In this case, we argue that the PPC tailored for the routing profile can greatly enhance the user-rate-reliability tradeoff.

Last, note that the primary user may also suffer from the random transmission outage, e.g., the collision due to the imperfect spectrum sensing of the CR user. Such damage appears in all *ad hoc* CRNs and is a function of spectrum sensing accuracy (more precisely, probability of missed detection), while the PPC technique proposed in this work aims at providing reliable communication for CR users. Nevertheless, the PPC technique can indirectly reduce the impact of the CR users to the primary users. For example, with the aid of the PPC technique, the CR users are able to successfully communicate in the ad hoc CRN with lower link availability, meaning that we can lower the energy detection threshold of the spectrum sensing. In this case, the probability of missed detection decreases, and thus the primary users are less likely collided with the CR users.

IV. Theoretical Error-Rate Analysis for PPC

To provide insight into the end-to-end PPC transmission in ad hoc CRNs, its performance is analyzed in this section. We first derive the PEP, which can be used to analyze BER and capacity. Due to the presence of erasures, the error rate cannot vanish even in the noise-free regime. Thus, the BER floor needs further investigation.

The PEP $f(x, \mathbf{r} \to \tilde{x}, \tilde{\mathbf{r}})$ is the probability of detecting the erroneous pair $(\tilde{x}, \tilde{\mathbf{r}})$ when transmitted PPC code word is $(x, \mathbf{r})$, which is formally defined as $f(x, \mathbf{r} \to \tilde{x}, \tilde{\mathbf{r}}) \triangleq P(\Lambda(x, \mathbf{r}, \tilde{x}, \tilde{\mathbf{r}}) < 0)$, where $\Lambda(x, \mathbf{r}, \tilde{x}, \tilde{\mathbf{r}})$ is the log-likelihood ratio (LLR), i.e., of $P(\mathbf{y}|x, \mathbf{r})$ and $P(\mathbf{y}|\tilde{x}, \tilde{\mathbf{r}})$:

$$\Lambda(x, \mathbf{r}, \tilde{x}, \tilde{\mathbf{r}}) \triangleq \log P(\mathbf{y} \mid x, \mathbf{r}, \mathbf{v}_{\mathbf{r}}) - \log P(\mathbf{y} \mid \tilde{x}, \tilde{\mathbf{r}}, \mathbf{v}_{\tilde{\mathbf{r}}}). \quad (11)$$

Since n_m is AWGN with noise power spectral density $N_{0,b}$, we obtain

$$P(\mathbf{y} \mid \mathbf{x}, \mathbf{r}, \mathbf{v}_{\mathbf{r}}) = \pi^{-M} \prod_{m=1}^{M} N_{0,b}^{-1} e^{-\frac{|y_m - h_{m,r_m} v_{m,r_m} x|^2}{N_{0,b}}}. \quad (12)$$

Inserting (12) to (11), we have

$$\Lambda(x, \mathbf{r}, \tilde{x}, \tilde{\mathbf{r}}) = \sum_{m=1}^{M} \frac{1}{N_{0,m}} \Big(|h_{m,r_m} v_{m,r_m} x - h_{\tilde{r}_m} v_{\tilde{r}_m} \tilde{x}|^2 + 2\mathrm{Re}\left\{ (h_{m,r_m} v_{m,r_m} x - h_{m,\tilde{r}_m} v_{m,\tilde{r}_m} \tilde{x})^* n_m \right\} \Big), \quad (13)$$

where $\mathrm{Re}\{\cdot\}$ denotes the real part, and $(\cdot)^*$ the complex conjugate. It can be seen from (13) that, conditioned on $(\mathbf{h}_{\mathbf{r}}, \mathbf{v}_{\mathbf{r}}, \mathbf{h}_{\tilde{\mathbf{r}}}, \mathbf{v}_{\tilde{\mathbf{r}}})$, $\Lambda(x, \mathbf{r}, \tilde{x}, \tilde{\mathbf{r}})$ is a Gaussian random variable with mean μ_Λ and variance σ_Λ^2 respectively given by

$$\mu_\Lambda = \sum_{m=1}^{M} \frac{1}{N_{0,m}} |h_{m,r_m} v_{m,r_m} x - h_{m,\tilde{r}_m} v_{m,\tilde{r}_m} \tilde{x}|^2, \quad \sigma_\Lambda^2 = 2\mu_\Lambda. \quad (14)$$

The moment-generating function (MGF) of the conditional Gaussian random variable Λ is given by

$$M_\Lambda(s \mid \mathbf{h_r}, \mathbf{v_r}, \mathbf{h_{\tilde{r}}}, \mathbf{v_{\tilde{r}}}) = e^{(s+s^2)\mu_\Lambda} m. \tag{15}$$

The unconditional MGF $M_\Lambda(s)$ then is represented as shown in (16) and (17), shown at the bottom of the page. The detail derivations is provided in Appendix.

Once $M_\Lambda(s)$ is obtained as shown in (16), we can analyze the diversity. We first assume that $P(v_{m,r}=1)=1$ for clarity. The Chernoff bound of the pair-wise error probability of the transmission pair $(x, \mathbf{r})$ and the erroneously-detected one $(\tilde{x}, \tilde{\mathbf{r}})$ is given by using the MGF in (16) and $s=\hat{s}$ for $(\log M_\Lambda(\hat{s}))'=0$ (Note that $(\cdot)'$ is the first-order derivative):

$$f_{\mathrm{CB}}(x, \mathbf{r}, \tilde{x}, \tilde{\mathbf{r}}) = M_\Lambda(\hat{s}) \approx \prod_{m=1}^{M} E_{|h_{m,r_m}x - h_{m,\tilde{r}_m}\tilde{x}|^2}\left\{ e^{-\frac{\left|h_{m,r_m}x - h_{m,\tilde{r}_m}\tilde{x}\right|^2}{4N_{0,b}}}, \right\}$$

where

$$E_{|h_{m,r_m}x - h_{m,\tilde{r}_m}\tilde{x}|^2}\left\{ e^{-\frac{\left|h_{m,r_m}x - h_{m,\tilde{r}_m}\tilde{x}\right|^2}{4N_{0,b}}} \right\} \approx \begin{cases} G_{N-1,1}^{1,N-1}\left[\frac{|x-\tilde{x}|^2}{4N_{0,m}} \middle| \begin{matrix} 0 & \cdots & 0 \\ & 0 & \end{matrix} \right], & \text{if } r_m = \tilde{r}_m, \\ G_{N,1}^{1,N}\left[\frac{(|x|^2+|-\tilde{x}|^2)}{4N_{0,b}} \middle| \begin{matrix} 0 & \cdots & 0 \\ & 0 & \end{matrix} \right], & \text{if } r_m \neq \tilde{r}_m. \end{cases}$$

From the above equations, we can see that the minimal diversity is $d_{\min}$ which occurs when $x=\tilde{x}$ and $\mathbf{r}\neq\tilde{\mathbf{r}}$. When the erasures are introduced, the diversity varies depending on the realizations of the erasures and becomes lower than $d_{\min}$.

Meanwhile, the PEP is computed by integration [28]

$$f(x, \mathbf{r} \to \tilde{x}, \tilde{\mathbf{r}}) = \frac{1}{2\pi j}\int_{\hat{s}-j\infty}^{\hat{s}+j\infty} M_\Lambda(s)\frac{\mathrm{d}s}{s}. \tag{18}$$

There exist a few approaches to tightly approximate this integral. Among these, we may use the Gaussian approximation, saddlepoint approximation [29], or the numerical Gauss-Chebyshev quadratures [30]. From the PEP, we can derive the BER P_{b} by applying the union bound [31]

$$P_{\mathrm{b}} \leq \frac{1}{|\chi|K\log_2(|\chi|K)} \sum_{\forall(x,\mathbf{r})} \sum_{\forall(\tilde{x},\tilde{\mathbf{r}})} d^{(b)}_{x,\mathbf{r},\tilde{x},\tilde{\mathbf{r}}} f(x, \mathbf{r} \to \tilde{x}, \tilde{\mathbf{r}}), \tag{19}$$

where $|\chi|$ is the cardinality of χ, and $d^{(b)}_{x,\mathbf{r},\tilde{x},\tilde{\mathbf{r}}}$ denotes the Hamming distance between the demapped bits of the code words $(x, \mathbf{r})$ and $(\tilde{x}, \tilde{\mathbf{r}})$. With the analytical BER, we can derive the capacity by assuming the PPC-coded channels equivalent to $|\chi|K$ binary symmetric channels with crossover probability $P_{\mathrm{b},l}$ of the lth channel, $l=1,\ldots,|\chi|K$. Since the BER of the lth bit can be obtained by using an approach similar to that used to derive (19), the associated capacity C can be computed as [32]

$$C = \sum_{l=1}^{\log_2(|\chi|K)} \log_2\left(2P_{\mathrm{b}}l^{P_{\mathrm{b}}l}(1-P_{\mathrm{b}}l)^{1-P_{\mathrm{b}}l}\right). \tag{20}$$

Last, due to the intrinsic randomness in *ad hoc* CRNs, the error rate of end-to-end PPC transmission cannot be vanishingly small even for infinitely large SNR. In fact, when all the R relay paths at all M time slots are erased, we have BER $=0.5$. Consequently, for a proper design of the PPC we need to investigate the BER floor. The data encoded by the path indices cannot be recovered if the erasures make $\mathbf{r}$ and $\tilde{\mathbf{r}}$ indistinguishable. For example, if $\mathbf{r}=[1,2,3,4]^\top$ and the erasures occur at the third and fourth relay paths at the third and fourth time instants, respectively, i.e., $v_{3,3}=0$ and $v_{4,4}=0$, the destination node cannot distinguish this case from the case of $\tilde{\mathbf{r}}=[1,2,4,3]^\top$ with $v_{3,4}=0$ and $v_{4,3}=0$, since both cases have the same path indices at the first and second time instants and erasures are detected at the third and fourth time instants. Define $r'=\arg\max_{r=1,\ldots,R} N_r$ and $\mathbf{b}'$ as the index vector where the kth element b'_k is associated with the index of the kth shortest waiting period. Then, for a permutation subset $\mathcal{C}_R(K, d_{\min})$, the largest probability of such error event is lower bounded by $\prod_{k=1}^{d_{\min}} P(v_{m'_k,r'}=0)$. Additionally, when erasures occur at all the $\mathbf{r}$ paths with lower bound probability

$$M_\Lambda(s) = E_{\mu_\Lambda}\left\{e^{(s+s^2)\mu_\Lambda}\right\} = \prod_{m=1}^{M} E_{|v_{m,r_m}h_{m,r_m}x - v_{m,\tilde{r}_m}h_{m,\tilde{r}_m}\tilde{x}|^2}\left\{ e^{\frac{s+s^2}{N_{0,b}}|v_{m,r_m}h_{m,r_m}x - v_{m,\tilde{r}_m}h_{m,\tilde{r}_m}\tilde{x}|^2} \right\} \tag{16}$$

$$E_{|v_{m,r_m}h_{m,r_m}x - v_{m,\tilde{r}_m}h_{m,\tilde{r}_m}\tilde{x}|^2}\left\{ e^{\frac{s+s^2}{N_{0,b}}|v_{m,r_m}h_{m,r_m}x - v_{m,\tilde{r}_m}h_{m,\tilde{r}_m}\tilde{x}|^2} \right\} \approx \begin{cases} P(v_{m,r}=0) + G_{N-1,1}^{1,N-1}\left[-\frac{(s+s^2)|x-\tilde{x}|^2}{N_{0,m}} \middle| \begin{matrix} 0 & \cdots & 0 \\ & 0 & \end{matrix} \right] P(v_{m,r}=1), & \text{if } r_m = \tilde{r}_m, \\ P(v_{m,r}=0)^2 + G_{N,1}^{1,N}\left[\frac{-(s+s^2)|x|^2}{N_{0,b}} \middle| \begin{matrix} 0 & \cdots & 0 \\ & 0 & \end{matrix} \right] P(v_{m,r}=0)P(v_{m,r}=1) + & \text{if } r_m \neq \tilde{r}_m, \\ G_{N,1}^{1,N}\left[\frac{-(s+s^2)|\tilde{x}|^2}{N_{0,b}} \middle| \begin{matrix} 0 & \cdots & 0 \\ & 0 & \end{matrix} \right] P(v_{m,r}=0)P(v_{m,r}=1) + G_{N,1}^{1,N}\left[\frac{-(s+s^2)\left(|x|^2+|-\tilde{x}|^2\right)}{N_{0,b}} \middle| \begin{matrix} 0 & \cdots & 0 \\ & 0 & \end{matrix} \right] P(v_{m,r}=1)^2, & \end{cases} \tag{17}$$

$\prod_{m=1}^{M} P(v_{m,r'}=0)$, x cannot be recovered, and the BER associated with x is 0.5. Based on these facts, the BER floor can be derived as

$$P_{\mathrm{m},N_{0,m}\to 0} \geq \frac{\prod_{k=1}^{d_{\min}} P\left(v_{m'_k,r'}=0\right)\log_2 K + \prod_{m=1}^{M} P\left(v_{m,r'}=0\right)\log_2|\chi|}{2\log_2\left(|\chi|+K\right)}, \tag{21}$$

which can be simplified to

$$P_{\mathrm{m},N_{0,m}\to 0} \geq \frac{P(v_{m,r}=0)^{d_{\min}}\log_2 K + P(v_{m,r}=0)^{M}\log_2|\chi|}{2\log_2\left(|\chi|+K\right)}, \tag{22}$$

if waiting periods of different time instants and the numbers of relay nodes in different relay paths are the same. As can be seen, the error floor not only depends on the erasure probability, but also is dominated by the diversity $d_{\min} \leq M$ of the end-to-end PPC transmission.

V. Decoding PPC

Using the MAP criterion for optimality, in this section we propose an efficient multiple-tree JSD to jointly identify the presence of erasures and decode the data packet.

A. MAP and Log-MAP Criteria

The MAP decoding criterion is expressed as follows:

$$\begin{aligned}(\hat{x},\hat{\mathbf{r}},\hat{\mathbf{v}}_{\hat{\mathbf{r}}}) &= \underset{x\in\chi,\mathbf{r}\in\mathcal{C}_R(K,d_{\min}),\mathbf{v}_{\mathbf{r}}\in\{0,1\}^M}{\arg\max} P(x,\mathbf{r},\mathbf{v}_{\mathbf{r}}\mid\mathbf{y}) \\ &= \underset{x\in\chi,\mathbf{r}\in\mathcal{C}_R(K,d_{\min}),\mathbf{v}_{\mathbf{r}}\in\{0,1\}^M}{\arg\max} \\ &\quad \times P(\mathbf{y}\mid x,\mathbf{r},\mathbf{v}_{\mathbf{r}})P(x)P(\mathbf{r})P(\mathbf{v}_{\mathbf{r}}),\end{aligned} \tag{23}$$

where $P(\mathbf{y}|x,\mathbf{r},\mathbf{v}_{\mathbf{r}})$ is given in (12). We assume that x and $\mathbf{r}$ are uniformly and randomly selected: x from χ with probability $P(\mathbf{x})=1/|\chi|$ for any x, and $\mathbf{r}$ from $\mathcal{C}_R(K,d_{\min})$ with probability $1/K$ for any $\mathbf{r}$, respectively. Since the erasures occur independently as shown in (2), the joint probability mass function (PMF) of the erasure vector $P(\mathbf{v}_{\mathbf{r}})$ is computed as $P(\mathbf{v}_{\mathbf{r}})=\prod_{m=1}^{M}P(v_{m,r_n})$. We then denote the LLR of v_{m,r_m} as $\Lambda(v_{m,r_m})=\log\frac{P(v_{m,r_m}=1)}{P(v_{m,r_m}=0)}$ so that $P(v_{m,r_m})=\frac{e^{v_{m,r_m}\Lambda(v_{m,r_m})}}{1+e^{\Lambda(v_{m,r_m})}}$. It is convenient, as it simplifies the computations and makes them more numerically stable, to use the logarithmic version of the MAP criterion (23). Then,

$$\begin{aligned}(\hat{x},\hat{\mathbf{r}},\hat{\mathbf{v}}_{\hat{\mathbf{r}}}) = \underset{x\in\chi,\mathbf{r}\in\mathcal{C}_R(K,d_{\min}),\mathbf{v}_{\mathbf{r}}\in\{0,1\}^M}{\arg\min} &\log P(\mathbf{y}\mid x,\mathbf{r},\mathbf{v}_{\mathbf{r}}) \\ &+\log P(x)+\log P(\mathbf{r})+\log P(\mathbf{v}_{\mathbf{r}}).\end{aligned} \tag{24}$$

Remove the irrelevant constant terms $-M\log\pi$, $-\log|\chi|$, $-\log K$, and $(1+e^{\Lambda(v_{m,r_m})})^{-1}$, $m=1,\ldots,M$. Then, assume that all relay paths have the same number of links, so that the subscript r_m of v_{m,r_m} can be omitted. By using such assumption, (24) can be represented as

$$(\hat{x},\hat{\mathbf{r}},\hat{\mathbf{v}}) \approx \underset{x\in\chi,\mathbf{r}\in\mathcal{C}_R(K,d_{\min}),\mathbf{v}\in\{0,1\}^M}{\arg\min} \mathcal{M}(x,\mathbf{r},\mathbf{v}) \tag{25}$$

with

$$\mathcal{M}(x,\mathbf{r},\mathbf{v})=\sum_{m=1}^{M}\frac{1}{N_{0,b}}\left|y_m-h_{m,r_m}v_b x\right|^2-\sum_{m=1}^{M}v_b\Lambda(v_b). \tag{26}$$

Note that this assumption simplifies the decoding procedure, since now the identification of the erasure vector $\mathbf{v}=[v_1,\ldots,v_M]$ is independent of the identification of $\mathbf{r}$. The search space of (25) is $(2^M-1)K|\chi|$, which is much smaller than $(2^{RM}-1)|\chi|^M$, the search space of the PTC decoding, thus proving the lower decoding complexity of the end-to-end PPC transmission.

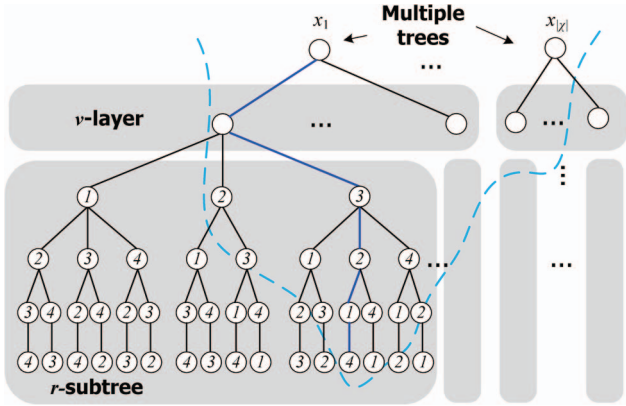

Fig. 4. Search structure of the proposed multiple-tree JSD. Each tree emanates from an $x\in\chi$ (the "root") and comprises a $\mathbf{v}$-layer and 2^M-1 $\mathbf{r}$-subtrees.

B. Multiple-Tree JSD

Sphere decoding (SD) is an efficient decoding algorithm that converts an exhaustive search into a constrained tree search [33]–[35] and is generally applied for spatial multiplexing MIMO transmission at physical layer. To apply this algorithm to the decoding of the end-to-end PPC transmission, we form $|\chi|$ tree searches as shown in Fig. 4, where each tree emanates from a specific constellation point in χ. From this root node, the $\mathbf{v}$-layer comprises 2^M-1 possible states of $\mathbf{v}$, excluding the null state $\mathbf{v}=\mathbf{0}$. The $\mathbf{r}$-subtree for the detection of $\mathbf{r}$ is cascaded below each node of the $\mathbf{v}$-layer. To traverse such multiple trees, the objective function $\mathcal{M}(x,\mathbf{r},\mathbf{v})$ (25) is rewritten in the form of an accumulation of partial distances (PDs) P_i: $\mathcal{M}(x,\mathbf{r},\mathbf{v})=\sum_{i=1}^{M+1}P_i$, where by using the descending index from the $\mathbf{v}$-layer to the bottommost layer of the subtree, the PDs P_i are defined as

$$\begin{aligned}P_{M+1} &= -\sum_{m=1}^{M}v_m\Lambda(v_m), \\ \sum_{i=1}^{M}P_i &= \left|y_m-h_{m,r_m}v_m x\right|^2.\end{aligned} \tag{27}$$

To enhance the decoding efficiency, the multiple-tree search is confined by d^2, where d is the radius. Once the accumulated

PDs from the $\mathbf{v}$-layer to the kth layer exceeds the value of d^2, i.e., $\sum_{i=k}^{M+1} D_i \geq d^2$, all nodes in the subtree inherited from that node are pruned out from the search space without affecting the search result of $(\hat{x}, \hat{\mathbf{r}}, \hat{\mathbf{v}})$. The radius is initialized by an arbitrarily large value, and gradually reduced during the tree search. In particular, if a leaf node, i.e., a node in the bottom-most layer, is visited, then the accumulated PDs of this node is used to update the radius, and hence shrink the search space. Note that the same update radius is applicable to all the $|\chi|$ tree searches, since the optimal $(\hat{x}, \hat{\mathbf{r}}, \hat{\mathbf{v}})$ has a single global minimum objective function.

Considering the example with $\mathcal{C}_4(16, 2)$ in Fig. 4. For a given $\mathbf{v}$ and x, the node number per subtree is reduced from 64 to 43, roughly a 33% reduction by using the tree formulation. If JSD with radius update is used, the number of nodes visited during the tree search is further reduced. Moreover, even if all nodes are visited, the number of PD calculations in the layers 1 to M is bounded by $(R+1)M$ for every tree rooted from a specific x. Specifically, given x, it is at most required to compute $|y_m|^2$ for $v_m = 0$, and $|y_m - h_{m,r_m} x|^2$ for $r_m = 1, \ldots, R$ and $v_m = 1$ at the bth layer. Last, it should be emphasized that, with the multiple-tree JSD, the receiver can gather probabilistic information about $\mathbf{v}$. By using this on-line learning process, the destination node can sense and track the variation of δ, which is particularly important when the channel statistics are time-varying.

VI. Numerical Examples

In this section, the performance of the end-to-end PPC transmission is evaluated, and the analysis is validated by means of Monte Carlo simulations. For simplicity and without much loss of generality, the noise power spectral density $N_{0,m}$ is assumed to be the same for all time instants. The adopted permutation subsets are chosen from those in Table I. For simplicity, we assume that the waiting periods W_m at various time instants $m = 1, \ldots, M$, and the number of opportunistic links N_r in various relay paths $r = 1, \ldots, R$, are the same, so we can omit their subscripts.

The reliability of the end-to-end transmission in *ad hoc* CRNs is degraded by noise and erasures. We first examine the error rate deterioration caused by noise in Fig. 5 with $\delta = 0$, implying that the links are always available. Such networks can also be regarded as a general class of ad hoc networks without erasures. The close agreement of analytical and numerical curves validates the accuracy of our theoretical analysis summarized by (19). The error rate performance is degraded for large N or small $d_{\min}$, which is the diversity of the end-to-end PPC transmission when the erasures are not considered as mentioned in Section IV. Nevertheless, without erasures, the error rate can be vanishingly small as the SNR increases. When the erasures are considered in Fig. 6, the error rate degrades, and an error floor appears. We set $\delta = 0.15$ based on the 15% spectrum utilization reported by FCC [36]. The case of double spectrum utilization $\delta = 0.3$ is also simulated to model the scenarios where the CR technology enhances the spectrum utilization. As can be seen, the numerical and analytical results are still matched.

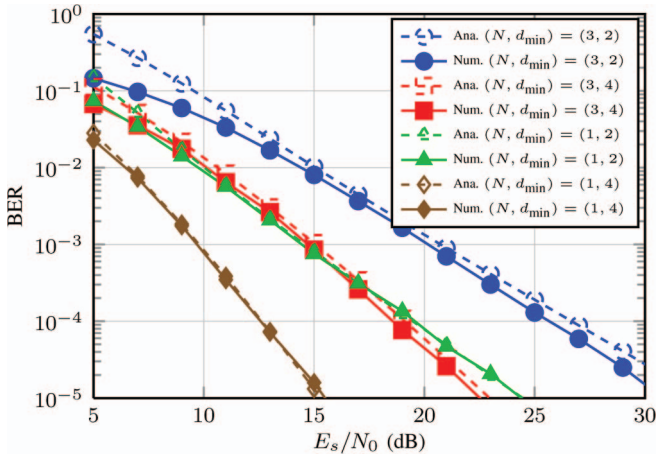

Fig. 5. Comparison of numerical and analytical BERs of end-to-end PPC transmission in ad hoc networks without transmission outage; QPSK, $\delta = 0$, and $R = 4$ are used.

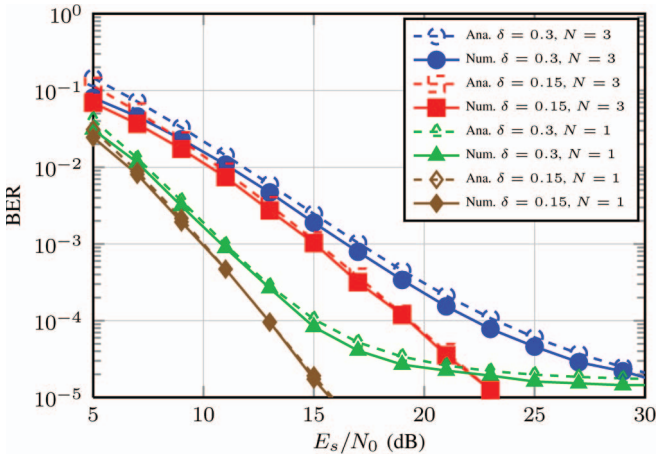

Fig. 6. Comparisons of numerical and analytical BERs of end-to-end PPC transmission in ad hoc CRNs; QPSK, $R = 4$ and $d_{\min} = 4$ are used; for $N = 1$ and $N = 3$, the waiting periods $W = 2$ and 6 are respectively used.

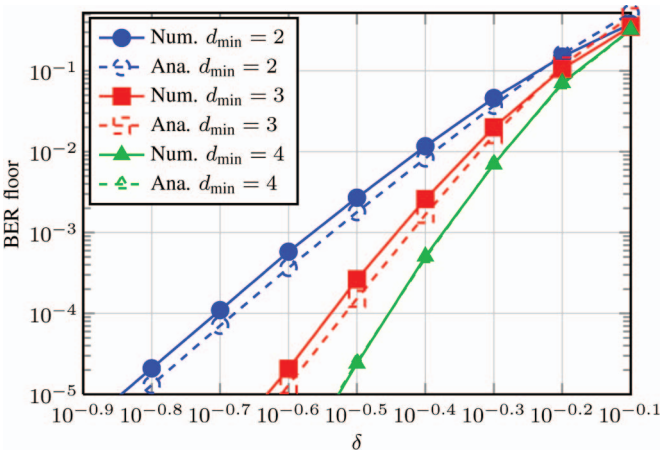

Fig. 7. Comparisons of numerical and analytical BER floors of the end-to-end PPC transmission; 16-QAM, $R = 4$, $N = 3$, and $W = 6$ are used.

To investigate the behavior of the error floors with various δ, Fig. 7 shows the numerical BER floor and its theoretical value derived in Section IV. The closely matched numerical and analytical results validate again our derivation. The slope of the

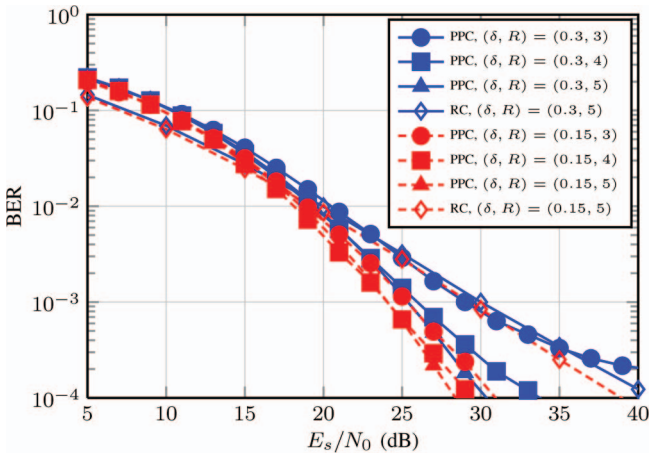

Fig. 8. BER of end-to-end transmission using various PPCs and repetition code (RC) with throughput 2 bits per time instant. 16-QAM and 64-QAM are respectively used for the end-to-end PPC transmission for the case of $R = 3$, 4 and the case of $R = 5$. QPSK is used for the end-to-end repetition code transmission for the case of $R = 5$. $N = 3$ and $W = 6$ are used.

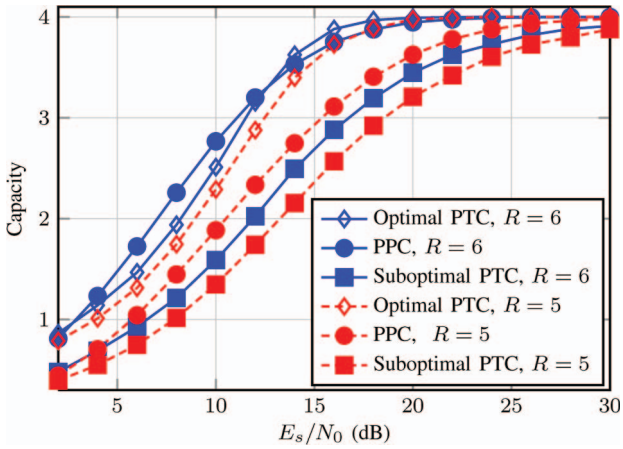

Fig. 9. Capacities of end-to-end transmission using various PPCs and PTC under a multiuser scenario with total throughput 4 bits per time instant. For $R = 5$ and $R = 6$, two and three users are considered, respectively. For $R = 5$, the end-to-end PPC transmission adopts 64-QAM and $K = 16$. For $R = 6$, two users apply end-to-end PPC transmission with 16-QAM and $K = 16$. End-to-end PTC transmission adopts 16-QAM and OSIC for suboptimal decoding. The values $\delta = 0.3$, $N = 3$, and $W = 6$ are used.

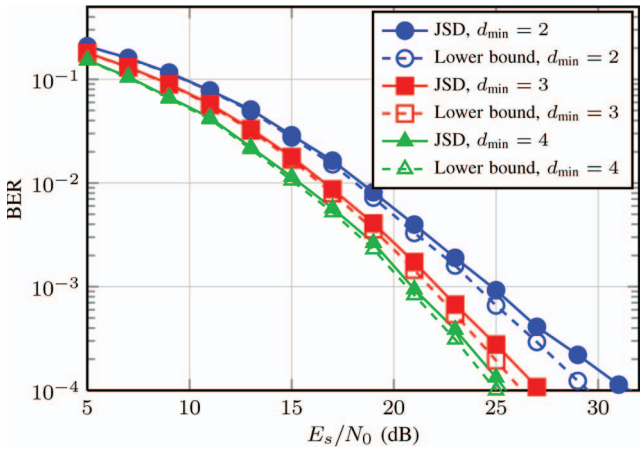

Fig. 10. BER of end-to-end PPC transmission using JSD. 16-QAM, $R = 4$, $\delta = 0.15$, $N = 3$, and $W = 6$ are used.

BER floor is dictated by the minimum Hamming distance $d_{\min}$, i.e., the diversity. Such results show that $d_{\min}$ is an essential design parameter for end-to-end PPC transmission. Now, under the same throughput, we numerically compare the BERs of the end-to-end transmission using PPC and the repetition code, where the latter transmission scheme sends the same x to all R paths (at each time instant). As shown in Fig. 8 for various numbers of relay paths and link unavailability, the BER of the end-to-end transmission using PPC is superior to that using the repetition code even when fewer relay paths are adopted. For the case of high link unavailability, that is, $\delta = 0.3$, the PPC performance enhancement achieved by using more relay paths and time instants is more pronounced.

To address the performance in a multiuser scenario, we investigate the sum rate of the end-to-end transmission, and compare PPC with PTC. Since PPC can be realized with low decoding complexity, we use ordered successive interference cancellation (OSIC) for suboptimal PTC decoding as a fair comparison. Let two and three users respectively access the same multipath routes for $R = 5$ and $R = 6$. As depicted in Fig. 9, in these two cases, the spectrum efficiencies of the end-to-end transmission using PPC are respectively 3 dB and 6 dB better than that using suboptimal PTC due to the PPC-based multiple access as introduced in Section III-B, while both schemes have a low decoding complexity. Even with one path less, the end-to-end PPC transmission still delivers a higher spectrum efficiency. Compared with the end-to-end PTC transmission with optimal but complicated decoding algorithm, the end-to-end PPC transmission achieves a comparable spectrum efficiency for the case of $R = 6$, with lower decoding complexity and control overhead for synchronization and multiple access.

Fig. 10 shows the BER of end-to-end transmission using the proposed multiple-tree JSD that realizes the optimal log-MAP criterion. The lower bound is obtained by assuming that the decoder has perfect knowledge of $\mathbf{V}$. Numerical results show that the proposed JSD delivers a BER generally close to the lower bound, demonstrating the effectiveness of this decoding algorithm.

For the comparison between the PPC and PTC transmissions, Fig. 11(a) depicts the BER comparison between the PTC transmission and PPC transmission with different values of $d_{\min}$. We can see that, with half of the spectrum efficiency per user, the PPC technique provides slightly better BER performance than the PTC technique. When the spectrum efficiency increases, The BER performance of the end-to-end PPC transmission degrades and becomes worse than that of the end-to-end PTC transmission. Fig. 11(b) depicts the number of visited nodes of the JSDs for the PPC and the PTC techniques. Compared with the exhaustive search that visits $(2^M - 1)K|\chi|$ nodes, the JSD of the PPC only requires at most 6%, 5%, and 3% number of visited nodes to deliver the MAP decoding performance. In addition to the identification of the erasures, the JSD of the PTC technique jointly decodes multiple coded packets, but the JSD of the PPC technique only decodes a single packet which includes the identification of the order of the accessed relay paths. Thus, the complexity per decoded bit of the PPC technique is much less than that of the PTC technique.

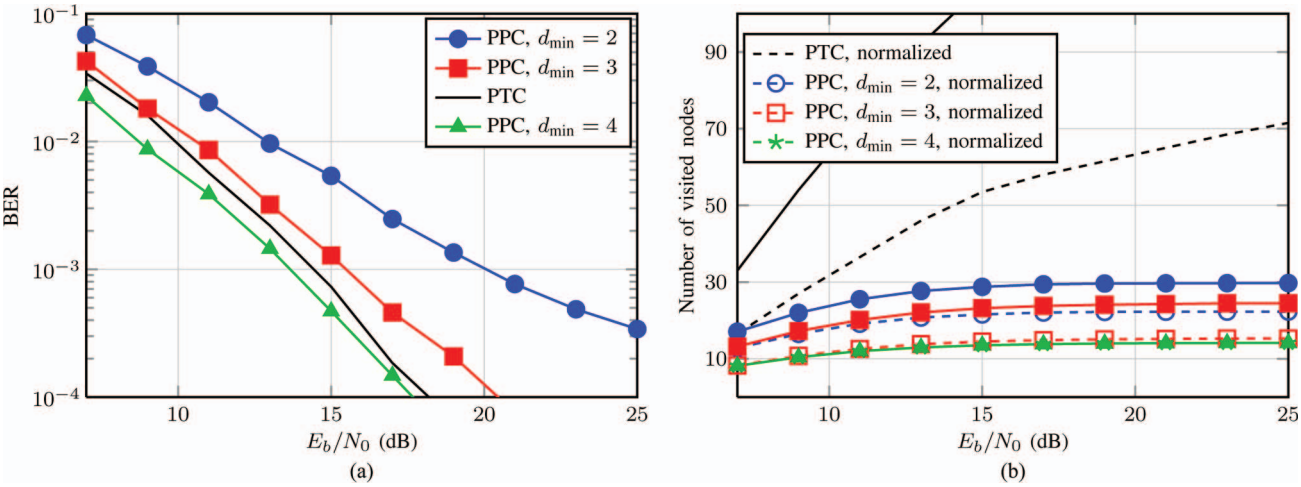

Fig. 11. Decoding complexity and error rate comparisons between the end-to-end PPC transmission and the end-to-end PTC transmission; QPSK, $R = 4$. (a) Error rate comparison. (b) Decoding complexity comparison.

VII. Conclusion

In this paper, we have introduced the PPC scheme for end-to-end transmission in *ad hoc* CRNs. The end-to-end PPC transmission hops among relay paths in the multipath routing, in which path selection is done according to the data to be transmitted. At the destination node, an efficient multiple-tree JSD algorithm based on the optimal log-MAP criterion is designed to jointly identify the erasures and decode the data. Since only one path is accessed, the end-to-end PPC transmission avoids control overheads of conventional multipath end-to-end transmission, caused by the synchronization of the arrival of multiple coded packets from multiple paths. We have provided theoretical analyses which shed light on the relationship among the design parameters. Comparing the PPC and the previously-proposed PTC techniques, numerical results demonstrate that, while the PTC technique is designed to optimize the performance of a single end-to-end transmission, the PPC technique delivers a higher spectrum efficiency in multiuser scenarios. Regarding the single-user case, the PPC technique also provides superior performance compared with the conventional repetition code scheme, along with simple decoding and low control overhead. Thus, we believe that the proposed end-to-end PPC transmission is suitable for multiuser scenarios in ad hoc CRN. The integration of PPC and PTC technologies in a single ad hoc CRN is an interesting direction for the future work.

Appendix

A. Derivation of MGF $M_\Lambda(s)$

To derive the unconditional MGF $M_\Lambda(s)$, we first average the random variables corresponding to the fading gains $(\mathbf{h_r}, \mathbf{h_{\tilde{r}}})$:

$$\begin{aligned} M_\Lambda(s) &= E_{\mathbf{h_r},\mathbf{v_r},\mathbf{h_{\tilde{r}}},\mathbf{v_{\tilde{r}}}}\left\{M_\Lambda(s \mid \mathbf{h_r}, \mathbf{v_r}, \mathbf{h_{\tilde{r}}}, \mathbf{v_{\tilde{r}}})\right\} \\ &= E_{\mu_\Lambda}\left\{e^{(s+s^2)\mu_\Lambda}\right\} = M_{\mu_\Lambda}(s+s^2), \end{aligned} \tag{28}$$

where $M_{\mu_\Lambda}(\cdot)$ denotes the MGF of the random variable μ_Λ. It follows that the problem of computing the MGF of Λ is reduced to calculating the MGF of μ_Λ.

To calculate $M_{\mu_\Lambda}(\cdot)$, let us first consider the pair of Bernoulli random variables $(\mathbf{v_r}, \mathbf{v_{\tilde{r}}})$. Depending on the values of $v_{m,r_m} \in \{0,1\}$ and $v_{m,\tilde{r}_m} \in \{0,1\}$, we may have four different values of $|h_{m,r_m} v_{m,r_m} x - h_{m,\tilde{r}_m} v_{m,\tilde{r}_m} \tilde{x}|^2$ in (13). Three of them give rise to the following values:

$$\begin{aligned} &|v_{m,r_m} h_{m,r_m} x - v_{m,\tilde{r}_m} h_{m,\tilde{r}_m} \tilde{x}|^2 \\ &\quad = \begin{cases} 0, & \text{if } (v_{m,r_m}, v_{m,\tilde{r}_m}) = (0,0), \\ |h_{m,r_m}|^2 |x|^2, & \text{if } (v_{m,r_m}, v_{m,\tilde{r}_m}) = (1,0), \\ |h_{m,\tilde{r}_m}|^2 |\tilde{x}|^2, & \text{if } (v_{m,r_m}, v_{m,\tilde{r}_m}) = (0,1). \end{cases} \end{aligned} \tag{29}$$

If $(v_{m,r_m}, v_{m,\tilde{r}_m}) = (1,1)$, two different sub-cases, depending on the relationship between r_m and $\tilde{r}_m$, need to be separately examined. If $r_m = \tilde{r}_m$, then

$$|h_{m,r_m} x - h_{m,\tilde{r}_m} \tilde{x}|^2 = |h_{m,r_m}|^2 |x - \tilde{x}|^2, \qquad r_m = \tilde{r}_m, \tag{30}$$

while, if $r_m \neq \tilde{r}_m$, the term $|h_{m,r_m} x - h_{m,\tilde{r}_m} \tilde{x}|^2$ can no longer be simplified. We shall approximate it as shown below.

To deal with $(\mathbf{h_r}, \mathbf{h_{\tilde{r}}})$, we observe that, since each link gain is an i.i.d. complex Gaussian random variable, $\mathbf{h_r}$ and $\mathbf{h_{\tilde{r}}}$ are products of complex Gaussian random variables. To simplify our derivation, we first assume that all relay paths have the same number of links, so that the subscript r of N_r can be removed. Next, define β_N as the random variable obtained as the square of the product of N Rayleigh random variables whose variances are normalized to unity. By normalizing the variances of the link gains, $|h_{m,r_m}|^2$ and $|h_{m,\tilde{r}_m}|^2$ for $m = 1, \ldots, M$ belong to this kind of random variables. Using the Meijer G-function, defined as

$$\begin{aligned} &G_{p,q}^{m,n}\left[x \,\middle|\, \begin{matrix} a_1 & \ldots & a_p \\ b_1 & \ldots & b_q \end{matrix}\right] \\ &\quad \triangleq \frac{1}{2\pi j} \int_{-j\infty}^{j\infty} \frac{\prod_{i=1}^{m} \Gamma(b_i + s) \prod_{i=1}^{n} \Gamma(1 - a_i - s)}{\prod_{i=m+1}^{q} \Gamma(1 - b_i - s) \prod_{i=n+1}^{p} \Gamma(a_i + s)} x^s \, \mathrm{d}s, \end{aligned} \tag{31}$$

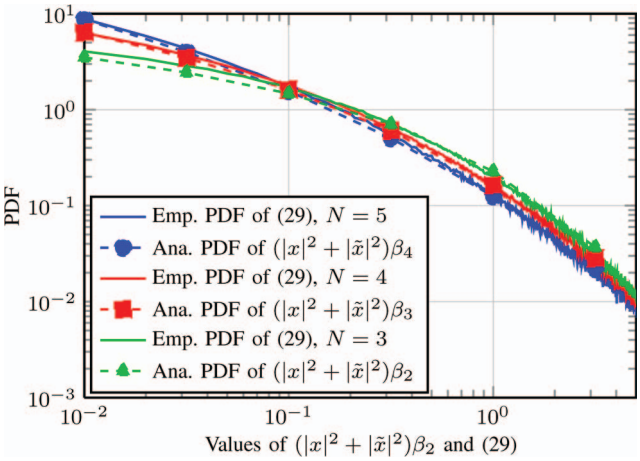

Fig. 12. The observation of the match between the analytical PDF of β_{N-1} and the empirical PDF of (29) when $(v_{m,r_m}, v_{m,\tilde{r}_m}) = (1,1)$ and $r_m \neq \tilde{r}_m$.

where $\Gamma(\cdot)$ is Gamma function, the probability density function (PDF) of β_N is expressed as [37]

$$f(\beta_N) = \beta_N^{-1} G_{0,N}^{N,0}\left[\beta_N \middle| \begin{matrix} -- \\ 1 \end{matrix} \begin{matrix} \\ \dots \end{matrix} \begin{matrix} \\ 1 \end{matrix}\right], \tag{32}$$

where, since $p=0$, the variables associated with a_p are represented by the dashes '$--$'. Then, using the integral [38]

$$\int_0^\infty x^{-\rho} e^{-\eta x} G_{p,q}^{m,n}\left[x \middle| \begin{matrix} a_1 \\ b_1 \end{matrix} \begin{matrix} \dots \\ \dots \end{matrix} \begin{matrix} a_p \\ b_q \end{matrix}\right] \mathrm{d}x = \eta^{\rho-1} G_{p+1,q}^{m,n+1}\left[\eta^{-1} \middle| \begin{matrix} \rho \\ \end{matrix} \begin{matrix} a_1 \\ b_1 \end{matrix} \begin{matrix} \dots \\ \dots \end{matrix} \begin{matrix} a_p \\ b_q \end{matrix}\right], \tag{33}$$

and letting variables ρ and η in (33) be 1 and $-s$, respectively, we compute the MGF of β_N as:

$$\begin{aligned} M_{\beta_N}(s) &= G_{1,N}^{N,1}\left[-s^{-1} \middle| \begin{matrix} \\ 1 \end{matrix} \begin{matrix} 1 \\ \dots \end{matrix} \begin{matrix} \\ 1 \end{matrix}\right] \\ &\overset{(a)}{=} G_{N,1}^{1,N}\left[-s \middle| \begin{matrix} 0 \\ \end{matrix} \begin{matrix} \dots \\ 0 \end{matrix} \begin{matrix} 0 \\ \end{matrix}\right], \end{aligned} \tag{34}$$

where (a) is due to [38]:

$$G_{q+1,p}^{p,1}\left[x^{-1} \middle| \begin{matrix} 1 \\ \end{matrix} \begin{matrix} b_1 \\ a_1 \end{matrix} \begin{matrix} \dots \\ \dots \end{matrix} \begin{matrix} b_q \\ a_p \end{matrix}\right] = \frac{\prod_{i=1}^q \Gamma(b_i)}{\prod_{i=1}^p \Gamma(a_i)} G_{p,q+1}^{1,p}\left[x \middle| \begin{matrix} \\ 0 \end{matrix} \begin{matrix} 1-a_1 \\ 1-b_1 \end{matrix} \begin{matrix} \dots \\ \dots \end{matrix} \begin{matrix} 1-a_p \\ 1-b_q \end{matrix}\right]. \tag{35}$$

Using the expression of the MGF of β_N in (34), we can derive the MGF of $|h_{m,r_m}x - h_{m,\tilde{r}_m}\tilde{x}|^2$ in (29) and (30), since $|h_{m,r_m}|$ and $|h_{m,\tilde{r}_m}|$ are both random variables obtained as the product of N Rayleigh random variables. However, for the case of $r_m = \tilde{r}_m$ and $(v_{m,r_m}, v_{m,\tilde{r}_m}) = (1,1)$, since we cannot further simplify $|h_{m,r_m}x - h_{m,\tilde{r}_m}\tilde{x}|^2$, the MGF in this case is hard to come by. Nevertheless, based on the empirical results depicted in Fig. 12, when h_{m,r_m} and $h_{m,\tilde{r}_m}$ are products of N complex Gaussian random variables, the PDF of $|h_{m,r_m}x - h_{m,\tilde{r}_m}\tilde{x}|^2$ can be approximated by the PDF of $(|x|^2 + |-\tilde{x}|^2)\beta_{N-1}$. Consequently, the MGF of μ_Λ in (28) can be reformulated as shown in (16).

REFERENCES

[1] J. Mitola, III, "Cognitive radio for flexible mobile multimedia communications," in *Proc. 6th IEEE Int. Workshop MOMUS Commun.*, Nov. 1999, pp. 3–10.

[2] J. Mitola, III and J. G. Q. Maguire, "Cognitive radio: Making software radios more personal," *IEEE Pers. Commun.*, vol. 6, no. 4, pp. 13–18, Aug. 1999.

[3] S. Haykin, "Cognitive radio: Brain-empowered wireless communications," *IEEE J. Sel. Areas Commun.*, vol. 23, no. 2, pp. 201–220, Feb. 2005.

[4] K.-C. Chen and R. Prasad, *Cognitive Radio Networks*. Chichester, U.K.: Wiley, 2009.

[5] E. Biglieri, A. J. Goldsmith, L. J. Greenstein, N. B. Mandayam, and H. V. Poor, *Principles of Cognitive Radio*. Cambridge, U.K.: Cambridge Univ. Press, 2013.

[6] K.-C. Chen *et al.*, "Routing for cognitive radio networks consisting of opportunistic links," *Wireless Commun. Mobile Comput.*, vol. 10, no. 4, pp. 451–466, Aug. 2009.

[7] A. Azarfar, J.-F. Frigon, and B. Sansò, "Improving the reliability of wireless networks using cognitive radios," *IEEE Commun. Surveys Tuts.*, vol. 14, no. 2, pp. 338–354, 2nd Quart. 2012.

[8] K. Yang and X. Wang, "Cross-layer network planning for multi-radio multi-channel cognitive wireless networks," *IEEE Trans. Commun.*, vol. 56, no. 10, pp. 1705–1714, Oct. 2008.

[9] L. Ding, T. Melodia, S. N. Batalama, J. D. Matyjas, and M. J. Medley, "Cross-layer routing and dynamic spectrum allocation in cognitive radio ad hoc networks," *IEEE Trans. Veh. Technol.*, vol. 59, no. 4, pp. 1969–1979, May 2010.

[10] M. Caleffi, I. F. Akyildiz, and L. Paura, "OPERA: Optimal routing metric for cognitive radio ad hoc networks," *IEEE Trans. Wireless Commun.*, vol. 11, no. 8, pp. 2884–2894, Apr. 2012.

[11] B. Mumey, J. Tang, I. R. Judson, and D. Stevens, "On routing and channel selection in cognitive radio mesh networks," *IEEE Trans. Veh. Technol.*, vol. 61, no. 9, pp. 4118–4128, Nov. 2012.

[12] K.-C. Chen and S. Lien, "Machine-to-machine communications: Technologies and challenges," *Ad Hoc Netw.*, vol. 18, pp. 3–23, Jul. 2013. [Online]. Available: http://www.sciencedirect.com/science/article/pii/S1570870513000395

[13] S.-C. Lin and K.-C. Chen, "Spectrum aware opportunistic routing in cognitive radio networks," in *Proc. IEEE GLOBECOM*, Dec. 2010, pp. 1–6.

[14] K. R. Chowdhury and I. F. Akyildiz, "CRP: A routing protocol for cognitive radio ad hoc networks," *IEEE J. Sel. Areas Commun.*, vol. 29, no. 4, pp. 794–804, Apr. 2011.

[15] Y. Liu, L. X. Cai, and X. Shen, "Spectrum-aware opportunistic routing in multi-hop cognitive radio networks," *IEEE J. Sel. Areas Commun.*, vol. 30, no. 10, pp. 1958–1968, Nov. 2012.

[16] P.-Y. Chen, W.-C. Ao, and K.-C. Chen, "Rate-delay enhanced multipath transmission scheme via network coding in multihop networks," *IEEE Commun. Lett.*, vol. 16, no. 3, pp. 281–283, Mar. 2012.

[17] M. K. Marina and S. R. Das, "On-demand multipath distance vector routing in ad hoc networks," in *Proc. IEEE ICNP*, Nov. 2001, pp. 14–23.

[18] P. Djukic and S. Valaee, "Reliable packet transmissions in multipath routed wireless networks," *IEEE Trans. Mobile Comput.*, vol. 5, no. 5, pp. 548–559, May 2006.

[19] S. Fashandi, S. O. Gharan, and A. K. Khandani, "Path diversity over packet switched networks: Performance analysis and rate allocation," *IEEE/ACM Trans. Netw.*, vol. 18, no. 5, pp. 1373–1386, May 2010.

[20] I-W. Lai, C.-H. Lee, and K.-C. Chen, "A virtual MIMO path-time code for cognitive ad hoc networks," *IEEE Commun. Lett.*, vol. 17, no. 1, pp. 4–7, Jan. 2013.

[21] I-W. Lai, C.-L. Chen, C.-H. Lee, K.-C. Chen, and E. Biglieri, "End-to-end virtual MIMO Transmission in ad hoc cognitive radio networks," *IEEE Trans. Wireless Commun.*, vol. 13, no. 1, pp. 330–341, Jan. 2014.

[22] I-W. Lai, C.-H. Lee, K.-C. Chen, and E. Biglieri, "Performance of path-time codes for end-to-end transmission in ad hoc multihop networks," in *Proc. IEEE ISIT*, Jun. 2014, pp. 66–70.

[23] Y. Jing and B. Hassibi, "Distributed space-time coding in wireless relay networks," *IEEE Trans. Wireless Commun.*, vol. 5, no. 12, pp. 3524–3536, Dec. 2006.

[24] W.-C. Ao and K.-C. Chen, "End-to-end HARQ in cognitive radio network," in *Proc. IEEE WCNC*, Jul. 2010, pp. 1–6.

[25] M. G. Khoshkholgh, K. Navaie, and H. Yanikomeroglu, "On the impact of the primary network activity on the achievable capacity of spectrum sharing over fading channels," *IEEE Trans. Wireless Commun.*, vol. 8, no. 4, pp. 2100–2111, Apr. 2009.

[26] E. Biglieri, *Coding for Wireless Channels*. New York, NY, USA: Springer-Verlag, 2005.
[27] H. C. Ferreira, A. J. H. Vinck, T. G. Swart, and I. de Beer, "Permutation trellis codes," *IEEE Trans. Commun.*, vol. 53, no. 11, pp. 1782–1789, Nov. 2005.
[28] G. Caire, G. Taricco, and E. Biglieri, "Bit-interleaved coded modulation," *IEEE Trans. Inf. Theory*, vol. 44, no. 3, pp. 927–946, May 1998.
[29] A. Martinez, A. Guillén i Fàbregas, and G. Caire, "Error probability analysis of bit-interleaved coded modulation," *IEEE Trans. Inf. Theory*, vol. 52, no. 1, pp. 262–271, Jan. 2006.
[30] E. Biglieri, G. Caire, G. Taricco, and J. Ventura-Traveset, "Simple method for evaluating error probabilities," *Electron. Lett.*, vol. 32, no. 3, pp. 191–192, Feb. 1996.
[31] M. Simon and M. S. Alouini, *Digital Communications Over Fading Channels*. Hoboken, NJ, USA: Wiley, 2005.
[32] J. Proakis and M. Salehi, *Digital Communications*, 5th ed. New York, NY, USA: McGraw-Hill, 2007.
[33] E. Viterbo and E. Biglieri, "A universal decoding algorithm for lattice codes," in *Proc. 14th GRETSI Symp.*, Juan les Pins, France, Sep. 1993, pp. 611–614.
[34] C. P. Schnorr and M. Euchner, "Lattice basis reduction: Improved practical algorithms and solving subset sum problems," *Math. Programm.*, vol. 66, no. 1–3, pp. 181–191, Aug. 1994.
[35] L. G. Barbero and J. S. Thompson, "Fixing the complexity of the sphere decoder for MIMO detection," *IEEE Trans. Wireless Commun.*, vol. 7, no. 6, pp. 2131–2142, Jun. 2008.
[36] *First Report and Order*, FCC Std. 02-48, Feb. 2002.
[37] J. Salo, H. M. El-Sallabi, and P. Vainkainen, "The distribution of the product of independent Rayleigh random variables," *IEEE Trans. Antennas Propag.*, vol. 54, no. 2, pp. 639–643, Feb. 2006.
[38] I. S. Gradshteyn and I. M. Ryzhik, *Table of Integrals, Series, and Products*, 7th ed. New York, NY, USA: Academic, 2007.

I-Wei Lai (M'11) received the Ph.D. degree in electrical engineering from the Graduate Institute of Electronics Engineering (GIEE), National Taiwan University in 2011. He worked with RWTH Aachen University, Germany, Academia Sinica, Taiwan, and Okayama University, Japan, in wireless communications. He was the recipient of the NTU-GIEE Best Thesis Award in 2011 for his Ph.D. thesis and is a member of Phi Tau Phi Scholastic Honor Society. His research interests include baseband signal processing, optimization, MIMO communication, and ad hoc cognitive radio network.

Chia-Han Lee received the B.S. degree from National Taiwan University, Taipei, Taiwan, in 1999, the M.S. degree from the University of Michigan, Ann Arbor, MI, USA, in 2003, and Ph.D. from Princeton University, Princeton, NJ, USA, in 2008, all in electrical engineering. From 1999 to 2001, he served in the R.O.C. army as a missile operations officer. From 2008 to 2009, he was a Postdoctoral Research Associate at the University of Notre Dame, Notre Dame, IN, USA. In 2010, he joined Academia Sinica as an Assistant Research Fellow, and since 2014, he has been an Associate Research Fellow in the same institute. His research interests include wireless communications and networks. He is an editor of IEEE TRANSACTIONS ON WIRELESS COMMUNICATIONS and IEEE COMMUNICATIONS LETTERS.

Kwang-Cheng Chen (M'89–SM'94–F'07) received the B.S. degree from the National Taiwan University in 1983, and the M.S. and Ph.D degrees from the University of Maryland, College Park, MD, USA, in 1987 and 1989, all in electrical engineering. From 1987 to 1998, he worked with SSE, COMSAT, IBM Thomas J. Watson Research Center, and National Tsing Hua University, in mobile communications and networks. Since 1998, He has been with National Taiwan University, Taipei, Taiwan, ROC, and is the Distinguished Professor and Associate Dean for academic affairs in the College of Electrical Engineering and Computer Science, National Taiwan University. He has been actively involved in the organization of various IEEE conferences as General/TPC chair/co-chair, and has served in editorships with a few IEEE journals. He also actively participates in and has contributed essential technology to various IEEE 802, Bluetooth, and LTE and LTE-A wireless standards. He is an IEEE Fellow and has received a number of awards such as the 2011 IEEE COMSOC WTC Recognition Award, 2014 IEEE Jack Neubauer Memorial Award and 2014 IEEE COMSOC AP Outstanding Paper Award. His recent research interests include wireless communications, network science, and data analytics.

Ezio Biglieri (M'73–SM'82–F'89–LF'10) was born in Aosta, Italy. He received the Dr. Engr. degree in electrical engineering from Politecnico di Torino, Italy, in 1967. He was elected three times to the Board of Governors of the IEEE Information Theory Society, and in 1999 he was the President of the Society. He is serving on the Scientific Board of the French company Sequans Communications, and, until 2012, he was a member of the Scientific Council of the "Groupe des Ecoles des Telecommunications" (GET), France. Since 2011, he has been a member of the Scientific Advisory Board of CHIST-ERA (European Coordinated Research on Long-term Challenges in Information and Communication Sciences & Technologies ERA-Net). In the past, he was Editor-in-Chief of the IEEE TRANSACTIONS ON INFORMATION THEORY, the IEEE COMMUNICATIONS LETTERS, the *European Transactions on Telecommunications*, and the *Journal of Communications and Networks*. Among other honors, he received the IEEE Donald G. Fink Prize Paper Award (2000), the IEEE Third-Millennium Medal (2000), the IEEE Communications Society Edwin Howard Armstrong Achievement Award (2001), the Journal of Communications and Networks Best Paper Award (2004 and 2012), the IEEE Information Theory Society Aaron D. Wyner Distinguished Service Award (2012), and the EURASIP Athanasios Papoulis Award "for outstanding contributions to education in communications and information theory" (2013).